



# Transcriptomics and Phenotyping Define Genetic Signatures Associated with Echinocandin Resistance in *Candida auris*

Sabrina Jenull,<sup>a,b</sup> Raju Shivarathri,<sup>c,d</sup> Irina Tsymala,<sup>a</sup> Philipp Penninger,<sup>a</sup>  Phan-Canh Trinh,<sup>a</sup> Filomena Nogueira,<sup>a,e</sup> Manju Chauhan,<sup>c,d</sup> Ashutosh Singh,<sup>f</sup> Andriy Petryshyn,<sup>a</sup> Anton Stoiber,<sup>a</sup>  Anuradha Chowdhary,<sup>f</sup>  Neeraj Chauhan,<sup>c,d</sup>  Karl Kuchler<sup>a</sup>

<sup>a</sup>Department of Medical Biochemistry, Max Perutz Labs Vienna, Medical University of Vienna, Campus Vienna Biocenter, Vienna, Austria

<sup>b</sup>Functional Microbiology, Institute of Microbiology, Department of Pathobiology, University of Veterinary Medicine, Vienna, Austria

<sup>c</sup>Public Health Research Institute, New Jersey Medical School, Rutgers, The State University of New Jersey, Newark, New Jersey, USA

<sup>d</sup>Department of Microbiology, Biochemistry and Molecular Genetics, New Jersey Medical School, Rutgers, The State University of New Jersey, Newark, New Jersey, USA

<sup>e</sup>CCRI-St. Anna Children's Cancer Research Institute, Vienna, Austria

<sup>f</sup>National Reference Laboratory for Antimicrobial Resistance in Fungal Pathogens, Medical Mycology Unit, Department of Microbiology, Vallabhbhai Patel Chest Institute, University of Delhi, Delhi, India

**ABSTRACT** *Candida auris* emerged as a human fungal pathogen only during the past decade. Remarkably, *C. auris* displays high degrees of genomic diversity and phenotypic plasticity, with four major clades causing hospital outbreaks with high mortality and morbidity rates. *C. auris* can show clinical resistance to all classes of antifungal drugs, including echinocandins that are usually recommended as first-line therapies for invasive candidiasis. Here, we exploit transcriptomics coupled with phenotypic profiling to characterize a set of clinical *C. auris* isolates displaying pronounced echinocandin resistance (ECN-R). A hot spot mutation in the echinocandin *FKS1* target gene is present in all resistant isolates. Moreover, ECN-R strains share a core signature set of 362 genes differentially expressed in ECN-R isolates. Among others, mitochondrial gene expression and genes affecting cell wall function appear to be the most prominent, with the latter correlating well with enhanced adhesive traits, increased cell wall mannan content, and altered sensitivity to cell wall stress of ECN-R isolates. Moreover, ECN-R phenotypic signatures were also linked to pathogen recognition and interaction with immune cells. Hence, transcriptomics paired with phenotyping is a suitable tool to predict resistance and fitness traits as well as treatment outcomes in pathogen populations with complex phenotypic diversity.

**IMPORTANCE** The surge in antimicrobial drug resistance in some bacterial and fungal pathogens constitutes a significant challenge to health care facilities. The emerging human fungal pathogen *Candida auris* has been particularly concerning, as isolates can display pan-antifungal resistance traits against all drugs, including echinocandins. However, the mechanisms underlying this phenotypic diversity remain poorly understood. We identify transcriptomic signatures in *C. auris* isolates resistant to otherwise fungicidal echinocandins. We identify a set of differentially expressed genes shared by resistant strains compared to unrelated susceptible isolates. Moreover, phenotyping demonstrates that resistant strains show distinct behaviors, with implications for host-pathogen interactions. Hence, this work provides a solid basis to identify the mechanistic links between antifungal multidrug resistance and fitness costs that affect the interaction of *C. auris* with host immune defenses.

**KEYWORDS** *Candida auris*, antifungal resistance, phenotypic variation, transcriptomics

The connection between the environment and human health is becoming increasingly clear. Climate change and human-imposed environmental destruction facilitate the emergence of new pathogens but also promote the development of antimicrobial drug

**Editor** Tom Chiller, CDC

**Copyright** © 2022 Jenull et al. This is an open-access article distributed under the terms of the [Creative Commons Attribution 4.0 International license](https://creativecommons.org/licenses/by/4.0/).

Address correspondence to Sabrina Jenull, jenulls@vetmeduni.ac.at, Neeraj Chauhan, chauhan1@njms.rutgers.edu, Anuradha Chowdhary, chowdhary.anuradha@gmail.com, or Karl Kuchler, karl.kuchler@meduniwien.ac.at.

The authors declare no conflict of interest.

**Received** 18 March 2022

**Accepted** 18 July 2022

resistance (1–3). The latter is further exacerbated by the extensive use and misuse of antimicrobials in agricultural, animal mass production, and clinical settings (4, 5). For instance, climate change may have promoted the emergence of the fungus *Candida auris* as a human pathogen, which was recently isolated from the natural marine environment in India (6, 7). *C. auris* was first identified in 2009 (8), and invasive infections were considered rare (9). However, over the last years, *C. auris* spread globally, causing outbreaks in health care facilities in more than 50 countries (10). Remarkably, *C. auris* emerged seemingly simultaneously at distinct geographical locations and is classified into four major phylogenetic clades (11). Furthermore, *C. auris* clades display substantial genetic diversity and show distinct phenotypic traits, especially diminished susceptibilities to antifungal therapies (11–14). For instance, the majority of all isolates, with the exception of clade II strains, are resistant to fluconazole (FCZ). Importantly, cross-resistance to drugs such as amphotericin B (AmB) and echinocandins (ECNs) is additionally occurring among isolates from distinct clades and geographical regions. Of note, numerous isolates displaying multidrug resistance (MDR) to two or all classes of antifungals have been recovered among clade I, clade III, and clade IV isolates (12, 13, 15, 16), with 41% of isolates displaying multidrug resistance and up to 4% displaying panresistance (10). Since ECN and AmB resistance can be rapidly acquired (17), the U.S. Centers for Disease Control and Prevention (CDC) highlighted *C. auris* as an urgent antibiotic resistance threat (18). Furthermore, diagnostic tools tailored to routine detection are scarce (19), and *C. auris* shows pronounced adhesion to abiotic and biotic surfaces such as human skin, thus facilitating human-to-human transmission in clinical settings (20).

The fungal cell wall plays pivotal roles in maintaining cellular integrity under normal as well as extreme environmental conditions (21). The cell wall architecture comprises the innermost chitin layer subtending glucan layers, with mannosylated proteins forming the outermost layers (22, 23). The fungicidal action of ECN is based on its inhibition of the *FKS* 1,3- $\beta$ -glucan synthase genes. Indeed, *FKS1* point mutations are commonly detected in ECN-resistant (ECN-R) *Candida* spp. (24, 25). Moreover, the cell wall, the first point of contact with the host (26), holds an array of pathogen-associated molecular patterns (PAMPs) engaging with host pattern recognition receptors (PRRs) that mediate pathogen recognition and antifungal effector mechanisms such as phagocytosis and the release of cytotoxic reactive oxygen species (ROS) (27). The structural features of cell wall mannose units vary among *C. auris* isolates, which is most likely affecting inflammatory host responses (28). In addition, host interaction or colonization abilities differ among *C. auris* clades (28, 29), underpinning the complex population structure of *C. auris*. However, the molecular mechanisms that facilitate the distinct biological properties of *C. auris* isolates remain elusive. While pioneering studies provided important insights into genomic plasticity (11, 13, 14), complementary studies are needed to explain the complex population structures driven by mechanisms beyond genomic diversity. Recently, studies exploiting transcriptomics, proteomics, and metabolomics have offered new insights into the molecular signatures of *C. auris* phenotypic diversity. For instance, transcriptional profiling of *C. auris* cells growing as cell aggregates revealed the increased transcription of certain cell wall-related genes compared to *C. auris* cells with nonaggregating phenotypes (30). Another comparative study explored the metabolomic, lipidomic, and proteomic differences of two *C. auris* isolates with distinct antifungal susceptibilities compared with *Candida albicans* (31). Of note, the extracellular vesicle contents of different isolates suggest distinct immunomodulatory properties (32). Recent work from our group demonstrated that specific transcriptional signatures correlate with phenotypic traits of *C. auris* patient isolates with opposing antifungal susceptibility profiles (33). Therefore, we further aimed to uncover additional signatures among clade I *C. auris* isolates with distinct phenotypic traits. Antifungal susceptibility profiling of clinical isolates identified a cluster of three ECN-R isolates, which were further compared to two other unrelated ECN-susceptible (ECN-S) strains using RNA sequencing (RNA-seq). Although all isolates are of clade I, large transcriptional alterations exist between ECN-R and ECN-S isolates under basal growth conditions, as a set of 362 genes was differentially expressed in all ECN-R

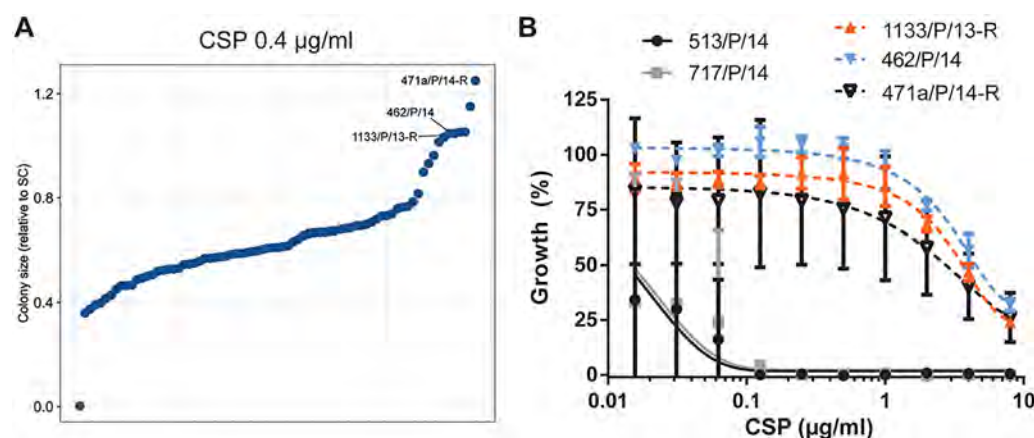


**FIG 1** Identification of caspofungin-resistant *C. auris* patient isolates. (A) Antifungal susceptibility screen on solid medium of clade I *C. auris* patient isolates. Cultures grown overnight in YPD medium at 30°C were spotted onto synthetic complete medium plates supplemented with caspofungin (CSP). Colony growth was imaged after 3 days of incubation at 30°C and used to assess the relative colony size (ratio of the colony size with an antifungal to that with no antifungal). The relative colony size was used to rank (CSP) susceptibilities among the tested isolates. Values represent the means from 3 biological replicates. (B) Confirmation of plate-based screening results using liquid growth inhibition assays. Cells were incubated in YPD medium with CSP at the indicated concentrations at 30°C for 24 h prior to OD<sub>600</sub> measurements. Data represent the means  $\pm$  SD from 3 biological replicates. (See also Fig. S1 in the supplemental material.)

isolates. These transcriptional profiles suggest distinct cell surface properties, reflected in the increased adhesion and enhanced host recognition of ECN-R isolates. Our work shows the utility of transcriptomic signatures to predict the phenotypic diversity of *C. auris* isolates and suggests that biological properties related to *C. auris* virulence may be reflected in certain subcluster traits.

## RESULTS

**Characterization of *C. auris* patient isolates.** The antifungal susceptibilities and MICs of *C. auris* can differ strikingly at both the inter- and intraclade levels (12, 14). Therefore, an automated antifungal testing pipeline can be useful for prescreening a larger set of clinical isolates to establish comparative antifungal susceptibility profiles. Recently, we analyzed the antifungal susceptibilities of 21 *C. auris* patient isolates belonging to clade I. We detected various antifungal susceptibility profiles (33), as also reported previously by others (12, 13). We included 64 additional clade I *C. auris* patient isolates and analyzed their susceptibility profiles on solid synthetic complete (SC) agar medium against antifungals representing all four major antifungal classes (see Materials and Methods; see also Fig. S1A to C in the supplemental material). The majority of clade I isolates displayed limited inhibition by FCZ and various susceptibilities to AmB (12). ECNs are recommended as first-line antifungal therapies against *C. auris* (34). Although resistance to ECN has been considered infrequent (35), recent reports suggest an ECN resistance rate of between 2 and 7% among *C. auris* isolates (12). Our screen identified isolates with limited caspofungin (CSP) susceptibilities, with isolate 471a/P/14-R being the least susceptible among the tested patient isolates (Fig. 1A). Moreover, we found two additional isolates that clustered with 471a/P/14-R based on the colony size reachable upon antifungal treatment (Fig. S1A, black box): 1133/P/13-R and 462/P/14. Like 471a/P/14-R, these isolates displayed low CSP susceptibility (Fig. 1A). Importantly, limited ECN susceptibility was reported for all 3 isolates in a previous study (36), thus confirming the robustness of our phenotyping. To delineate the conserved mechanisms mediating decreased CSP efficacy, we set out to further characterize these isolates in comparison to CSP-susceptible isolates. We chose isolates 513/P/14 and 717/P/14 as they displayed otherwise similar antifungal susceptibility profiles (Fig. S1A, marked with asterisks). Since the above-described solid-medium robotic screen is not a validated or clinically approved method for antifungal susceptibility testing, we confirmed the decreased growth inhibition upon CSP treatment of isolates

**TABLE 1** MIC values as determined by the CSLI broth microdilution method<sup>a</sup>

Isolate	Source	Hospital/yr of isolation	MIC ( $\mu\text{g/mL}$ )									
			ICZ	VCZ	ISZ	PSZ	AmB	CSP	MFG	AFG	FCZ	5FC
1133/P/13-R	Blood	Hosp1/2013	0.5	2	0.5	0.25	8	8	8	8	64	0.5
462/P/14	Blood	Hosp2/2014	0.125	1	0.25	0.015	0.5	4	8	8	64	0.5
471a/P/14-R	Blood	Hosp2/2014	0.25	1	0.125	0.015	0.5	8	8	8	64	0.5
513/P/14	Blood	Hosp3/2014	2	4	2	1	4	1	0.25	0.5	64	0.25
717/P/14	Tissue	Hosp1/2014	0.125	2	0.125	0.015	4	0.25	0.125	0.125	64	32

<sup>a</sup>ICZ, itraconazole; VCZ, voriconazole; ISZ, isavuconazole; PSZ, posaconazole; AmB, amphotericin B; CSP, caspofungin; MFG, micafungin; AFG, anidulafungin; FCZ, fluconazole; 5FC, 5-flucytosine.

471a/P/14-R, 1133/P/13-R, and 462/P/14 in liquid yeast extract-peptone-dextrose (YPD) medium in comparison to the susceptible isolate controls 513/P/14 and 717/P/14. Of note, all five isolates displayed comparable AmB and FCZ susceptibilities (Fig. S1D and E). In addition, MIC assays according to Clinical and Laboratory Standards Institute (CLSI) protocols further verified the low CSP susceptibilities of isolates 471a/P/14-R, 1133/P/13-R, and 462/P/14 (Table 1). Additionally, other ECNs such as micafungin (MFG) and anidulafungin (AFG) exerted limited growth inhibition against 471a/P/14-R, 1133/P/13-R, and 462/P/14. Based on CDC-suggested breakpoints for ECNs (MICs of  $>4 \mu\text{g/mL}$  for AFG and MFG and  $>2 \mu\text{g/mL}$  for CSP [37]), these isolates can be considered ECN-R, as pointed out previously (36).

**ECN-R isolates display distinct transcriptomic profiles.** To better understand whether ECN-R isolates share additional characteristics that make them distinguishable from ECN-S isolates, we further characterized these isolates at the molecular level. Therefore, we performed comparative transcriptomics analyses of ECN-R and ECN-S isolates grown in liquid YPD medium at 30°C. A principal-component analysis (PCA) of normalized read counts demonstrated that ECN-R (471a/P/14-R, 1133/P/13-R, and 462/P/14) and ECN-S (513/P/14 and 717/P/14) isolates display distinct transcriptomes (Fig. 2A) (PC1, 38% variance). This was further reflected by the high number of differentially expressed genes (DEGs), which affected 24 to 12% of all detected *C. auris* coding sequences (CDSs) being at least 1.5-fold up- or downregulated in ECN-R compared to ECN-S isolates (Table 2). Interestingly, only 93 genes, representing 2% of *C. auris* CDSs (detected by RNA-seq here), were deregulated between two independent ECN-S isolates, 513/P/14 and 717/P/14 (Table 2). In comparison, 7% of detected CDSs were differentially expressed between the ECN-R isolates 462/P/14 and 471a/P/14-R (Table 2), with the latter forming a subcluster among ECN-R isolates (Fig. 2A). Yet the total number of DEGs is more than 3-fold smaller when 471a/P/14-R is compared to ECN-S isolates. For instance, 1,192 and 1,284 genes were differentially expressed in 471a/P/14-R with respect to the ECN-S 717/P/14 and 513/P/14 controls, respectively. In comparison, altered expression of 356 genes was detected between ECN-R isolates 471a/P/14-R and 462/P/14 (Table 2). As we observed a substantial number of DEGs, we further assessed whether the direction of transcriptional deregulation (up- or downregulated) is conserved in ECN-R isolates compared to both ECN-S isolates. Therefore, we directly compared the fold changes (FCs) in gene expression between one ECN-R isolate and both ECN-S strains (i.e., 1133/P/13-R versus 513/P/14 and 1133/P/13-R versus 717/P/14), demonstrating a high correlation of deregulated genes ( $R \geq 0.88$ ) (Fig. 2B and Fig. S2A and B). Gene ontology (GO) analysis of DEGs (false discovery rate [FDR] of  $<0.05$ ;  $>1.5$ -fold change) further revealed that related biological processes are commonly deregulated in ECN-R isolates compared to each ECN-S *C. auris* isolate (Fig. 2C and Table S4). For instance, genes associated with mitochondrial gene expression (adjusted *P* value of  $4.49 \times 10^{-05}$ ) were commonly enriched in all resistant versus susceptible strains (Fig. 2C), showing predominantly enhanced expression in ECN-R strains (Fig. S2C). Accordingly, 579 or 474 common genes were differentially regulated among all ECN-R isolates compared to ECN-S isolate 513/P/14 or 717/P/14, respectively (Fig. S2D and E). These common DEGs represent 34% and 30% of all DEGs from ECN-R-versus-513/P14 (579 out of 1,702) and ECN-R-versus-717/P/14 (474 out of 1,559) comparisons, respectively. Collectively, the related transcriptomic alterations and similar biological processes affected between ECN-R and ECN-S isolates, as well as the



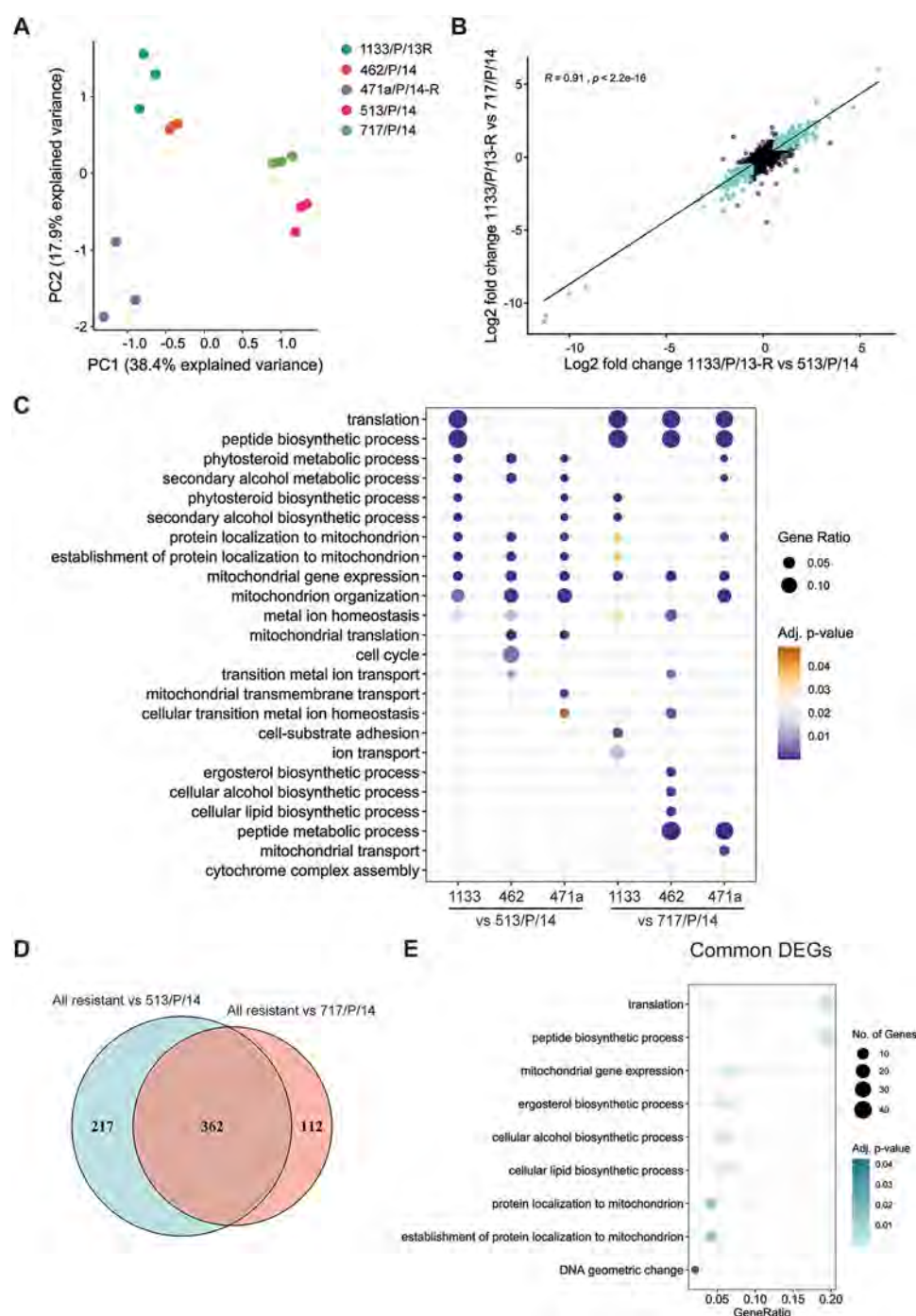


**FIG 2** Transcriptional profiles of ECN-R and ECN-S patient isolates. (A) Principal-component analysis (PCA) based on normalized RNA-seq read counts (counts per million [CPM]). (B) Scatterplot depicting the log<sub>2</sub> fold changes in transcript abundances for the indicated pairwise comparisons. The Pearson correlation coefficient ( $R$ ) and linear regression line are indicated. Turquoise dots represent common differentially expressed genes (DEGs) (FC of >1.5; FDR of <0.05) in both comparisons. (C) GO enrichment analysis of DEGs (FC of >1.5; FDR of <0.05) for the indicated comparisons. The dot size represents the gene ratio, meaning the number of genes enriched in the plotted GO term relative to the total number of DEGs used as the input data. Due to space reasons, 1133/P/13-R, 462/P/14, and 471a/P/14-R are abbreviated 1133, 462, and 471a, respectively. (D) Venn diagram depicting the overlap of common genes differentially expressed (FDR of <0.05; FC of >1.5) between all ECN-R isolates (471a/P/14-R, 1133/P/13-R, and 462/P/14 ["All resistant"]) and ECN-S isolates 513/P/14 and 717/P/14. (E) GO enrichment analysis of common DEGs between all ECN-R isolates and both ECN-S isolates (Venn diagram intersection in panel D). The gene ratio represents the number of genes enriched in the plotted GO term relative to the total number of DEGs used as the input data. The dot size reflects the number of genes enriched in the corresponding GO term. (See also Fig. S2 in the supplemental material.)

**TABLE 2** Differentially expressed genes in comparisons of ECN-R versus ECN-S isolates<sup>a</sup>

Comparison	Resistance	No. of genes			
		Upregulated	Downregulated	Total	% of total genes
1133/P/13-R vs 513/P/14	ECN-R vs ECN-S	645	497	1,142	21
462/P/14 vs 513/P/14	ECN-R vs ECN-S	496	308	804	15
471a/P/14-R vs 513/P/14	ECN-R vs ECN-S	755	529	1,284	24
1133/P/13-R vs 717/P/14	ECN-R vs ECN-S	507	452	959	18
462/P/14 vs 717/P/14	ECN-R vs ECN-S	368	305	673	12
471a/P/14-R vs 717/P/14	ECN-R vs ECN-S	668	524	1,192	22
513/P/14 vs 717/P/14	ECN-S vs ECN-S	12	81	93	2
462/P/14 vs 471a/P/14-R	ECN-R vs ECN-R	190	166	356	7

<sup>a</sup>The ECN-R isolates were 1133/P/13-R, 462/P/14, and 471a/P/14-R. The ECN-S isolates were 513/P/14 and 717/P/14. The cutoffs were an FDR of <0.05 and a log<sub>2</sub> fold change of >0.58.

substantial overlap of DEGs, suggest a core signature gene set linked to ECN-R traits in unrelated isolates. Therefore, we next aimed to define the core set of common DEGs between ECN-R and ECN-S *C. auris* isolates. We identified a set of 362 DEGs shared among all three ECN-R isolates, compared to both ECN-S isolates (Fig. 2D), and denoted them ECN-R core genes. Functionally, core genes were linked to three major biological functions, including translation (adjusted *P* value of  $4.91 \times 10^{-09}$ ), ergosterol biosynthetic processes (adjusted *P* value of  $4.91 \times 10^{-09}$ ), and mitochondrial gene expression (adjusted *P* value of  $1.12 \times 10^{-07}$ ), as revealed by GO enrichment analysis (Fig. 2E and Table S4). Genes linked to mitochondrial gene expression and function included mitochondrial translation initiation and elongation factors (*IFM1* and *TUF1*, respectively) as well as several mitochondrial ribosomal proteins (e.g., *RSM4*, *MRPL36*, B9J08\_000156, and B9J08\_000569) (Table S4; see also Table S3 for *C. auris* gene identifiers). Additionally, genes implicated in mitochondrial protein import (*TOM70*, *TOM40*, *TOM22*, *TIM50*, *TIM44*, *TIM40*, and *TIM23*) were upregulated in all ECN-R isolates (see Table S3 for *C. auris* gene identifiers), suggesting altered mitochondrial function in ECN-R isolates. Therefore, we tested the susceptibility of ECN-R strains to the respiratory chain inhibitor antimycin A (38). Indeed, the ECN-R isolates displayed roughly 2- to 3-fold-decreased antimycin A 50% inhibitory concentration (IC<sub>50</sub>) values compared to the ECN-S isolates (Fig. S2F). In summary, these data demonstrate that ECN-R isolates show distinct transcriptional profiles, affecting about 6% of all *C. auris* genes (362 out of 5,397 *C. auris* genes detected here).

**ECN-R isolates have altered cell surface properties.** The mechanisms and modulators of ECN susceptibility have been explored in other *Candida* spp. such as *C. albicans* and *C. glabrata* (39–44). To assess whether genes previously implicated in CSP susceptibility in *C. albicans* are also regulated in *C. auris* ECN-R isolates, we retrieved the relevant genes from the *Candida* Genome Database (CGD) (<http://www.candidagenome.org/>), which contained 110 genes. We then assessed the expression of the corresponding *C. auris* homologues in ECN-R versus ECN-S isolates. For instance, we found 20 genes differentially regulated in ECN-R isolate 1133/P/13-R compared to ECN-S isolate 513/P/14 (Fig. 3B). Of note, the ECN targets *FKS1* and *FKS2* were not differentially regulated at the mRNA level (Fig. S3A). However, three genes known to modulate CSP susceptibility in *C. albicans* were commonly deregulated in all ECN-R *C. auris* isolates compared to both ECN-S isolates (Fig. S3C). These genes included the transcription factor *NRG1* (B9J08\_005429), the kinase *GIN4* (B9J08\_005249), and the cell wall-associated gene *PGA31* (B9J08\_000117) (Fig. S3C). As alterations in the cell wall architecture impact CSP susceptibility (45), we further inspected genes related to cell wall function (GO cellular component annotation containing “cell wall”) among the core set in ECN-R isolates. Thereby, we identified 16, predominantly downregulated, genes in ECN-R isolates (Fig. 3A). Similarly, gene set enrichment analysis (GSEA) revealed the enrichment of fungal-type cell wall genes among the differentially expressed ECN-R core genes (Fig. 3B). Among the regulated cell wall genes were homologues of *C. albicans* glucanase genes (*XOG1* and *ENG1*) (46, 47) as well as genes encoding putative adhesins (*ALS4*, *IFF4*, and *PGA6*) (48–50). These data suggest that ECN-R isolates harbor altered cell wall structure and surface properties. Indeed, ECN-R *C. auris* isolates showed

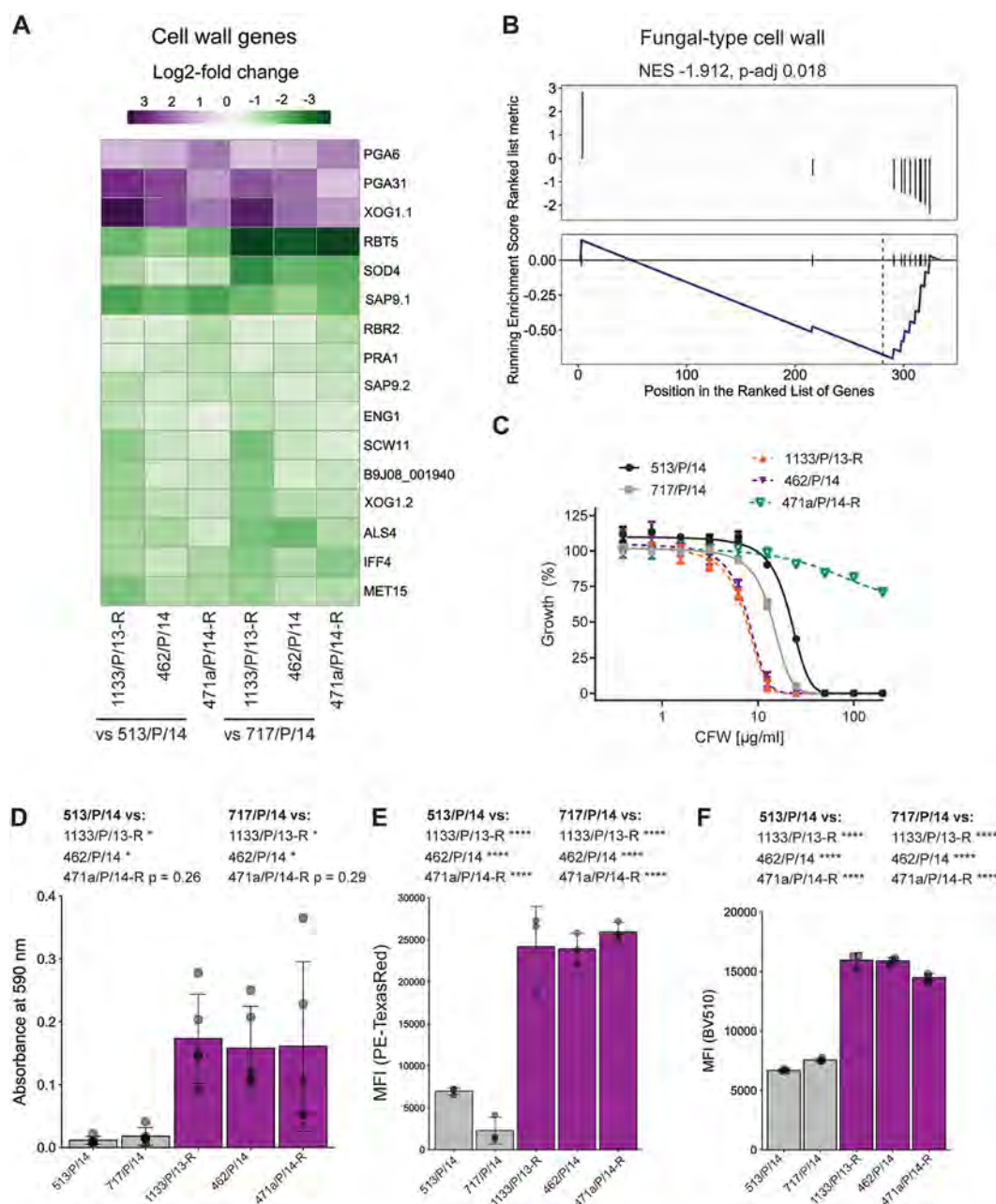


**FIG 3** ECN-R isolates show altered cell surface properties. (A) Heatmap depicting log<sub>2</sub> fold changes of genes that contain "cell wall" in the fungal-type cellular component GO term category and that are commonly differentially expressed (FDR of <0.05; FC of >1.5) between all ECN-R isolates and both ECN-S *C. auris* isolates. Gene names refer to *C. albicans* homologues. Notably, two *C. auris* genes were found to be homologous to *C. albicans* *XOG1* and *SAP9*. Those genes are depicted as *XOG1.1* and *XOG1.2* and *SAP9.1* and *SAP9.2*, respectively. *C. auris* gene identifiers are depicted if no gene name was annotated to the *C. albicans* homologue. Table S5 in the supplemental material presents the gene list and the corresponding identifiers. (B) Commonly differentially expressed genes between ECN-R and ECN-S isolates were ranked according to their log<sub>2</sub> fold changes between 1133/P/13-R and 513/P/14 and subjected to gene set enrichment analysis (GSEA). The plot depicts the ranked gene list (top) and the enrichment score (bottom) for the GO term category "fungal-type cell wall." (C) Growth inhibition in liquid YPD medium in response to calcofluor white (CFW) at the indicated concentrations. OD<sub>600</sub> values were measured after 24 h at 30°C. The percentage of growth upon CFW treatment relative to growth in YPD medium is depicted. Data represent the means and SD from three biological replicates. (D) Adhesion to plastic as assessed by crystal violet staining after 4 h of static YPD culture in polystyrene plates at 37°C. Mean values and SD from 5 biological replicates are plotted. (E) Concanavalin A-Texas Red staining of *C. auris* cells grown to the exponential growth phase in YPD medium at 30°C. The mean fluorescence intensity (MFI) is depicted. Data represent the means and SD from 3 biological replicates. (F) Aniline blue staining of *C. auris* cells grown as described above for panel E. The MFI is depicted, and data represent the means plus SD from 3 biological replicates. \*,  $P < 0.05$ ; \*\*\*\*,  $P < 0.00001$  (by one-way ANOVA and Tukey's multiple-comparison test for the indicated comparisons). Statistical homoscedasticity of the data was assessed by Bartlett's test. The data presented in panel D were heteroscedastic, and hence, Welch's ANOVA was applied. NES, normalized enrichment score. (See also Fig. S3.)

enhanced adhesion to plastic and differential susceptibilities to the cell wall-perturbing agent calcofluor white (CFW) (Fig. 3C and D). Notably, adhesive properties were variable for isolate 471a/P/14-R, which also showed decreased sensitivity to CFW, while 1133/P/13-R and 462/P/14 were more susceptible to CFW treatment than the ECN-S isolates (Fig. 3C). Finally, we confirmed the differences in cell wall composition between ECN-S and ECN-R isolates, with the latter showing increased mannan and  $\beta$ -glucan contents (Fig. 3E and F). Notably, the exposure of  $\beta$ -glucans was slightly decreased compared to that of the susceptible control isolate 513/P/14. However, the same trend was also seen when 513/P/14 was compared to ECN-S isolate 717/P/14. The chitin abundance was unaltered among the isolates (Fig. S3E).

The fungal cell wall is a dynamic structure that is affected by environmental conditions (51) and alterations in the abundances of cell wall-modulating enzymes (52, 53) and mannosylated proteins (54). *PGA6* (B9J08\_001366), a homologue of a putative *C. albicans* glycosylphosphatidylinositol (GPI)-anchored adhesion molecule (49), was among the upregulated cell wall-related genes in ECN-R isolates, in addition to Putative GPI-anchored protein (*PGA31*) and the exoglucanase gene *XOG1* (46) (Fig. 3A). Interestingly, the ectopic overexpression or deletion of other PGA family proteins affects fungal adhesion as well as CSP sensitivity (45, 54), and *PGA6* was found to be upregulated in CSP-treated *C. auris* cells (55). Therefore, we constructed a deletion mutant lacking *PGA6* to test whether it contributes to ECN-R and adhesion in *C. auris*. However, the loss of *PGA6* in ECN-R isolates 471a/P/14-R, 1133/P/13-R, and 462/P/14 only moderately reduced adhesion (Fig. S3E) and did not affect CSP susceptibility (Fig. S3F).

**ECN-R isolates trigger enhanced macrophage responses.** In addition to glucans, mannans are major drivers of host responses to *C. auris* (28). Since we detected major mannan increases in ECN-R isolates, we next assessed whether this affects host interactions with primary murine bone marrow-derived macrophages (BMDMs). We chose isolate 717/P/14 as a representative of ECN-S isolates and the ECN-R isolates 1133/P/13-R and 462/P/14. Fungal coculture experiments showed that the rate of phagocytosis of fluorescein isothiocyanate (FITC)-labeled ECN-R isolates was approximately 2-fold higher for 717/P/14 after 45-min and 120-min interactions with BMDMs (Fig. 4A and B). In addition, the release of reactive oxygen species (ROS) was diminished upon challenge with ECN-S isolate 717/P/14 compared to the responses to ECN-R isolates (Fig. 4C and Fig. S4C). However, killing by BMDMs was slightly enhanced for 717/P/14 cells after 4 h of coculture (Fig. 4D). Notably, ECN-S isolate 717/P/14 displayed an elevated growth rate under BMDM culture conditions compared to ECN-R isolates 1133/P/13-R and 462/P/14 (Fig. S4B). However, the fungal viability in cocultures with BMDMs was calculated relative to that of *C. auris* cultured without immune cells (see Materials and Methods) to minimize bias due to differential fungal growth under BMDM culture conditions. Collectively, these data demonstrate distinct phenotypic, transcriptomic, and antifungal host responses of ECN-R and ECN-S *C. auris* isolates. ECN-R traits are linked to a shared set of commonly dysregulated genes in *C. auris* isolates, suggesting that such transcriptomic fingerprints could be helpful for predicting antifungal resistance and virulence-related traits in *C. auris*.

## DISCUSSION

In addition to environmental stress, pathogens can face severe challenges by host immune defenses or therapeutic intervention strategies such as antibiotic or antifungal treatment (56). Phenotypic plasticity facilitating stress adaptation is therefore key for microbial survival. Multiple mechanisms enable adaptive traits, including genomic alterations or epigenetic modifications that govern transcriptional and phenotypic adaptation (57). The evolutionary diversification of *C. auris* and its emergence as a human pathogen are still poorly understood (58). Molecular clock analyses estimate that the last common ancestor for each *C. auris* clade arose within the last 360 years. In contrast, simultaneous clade diversification may have happened more recently (13). Of



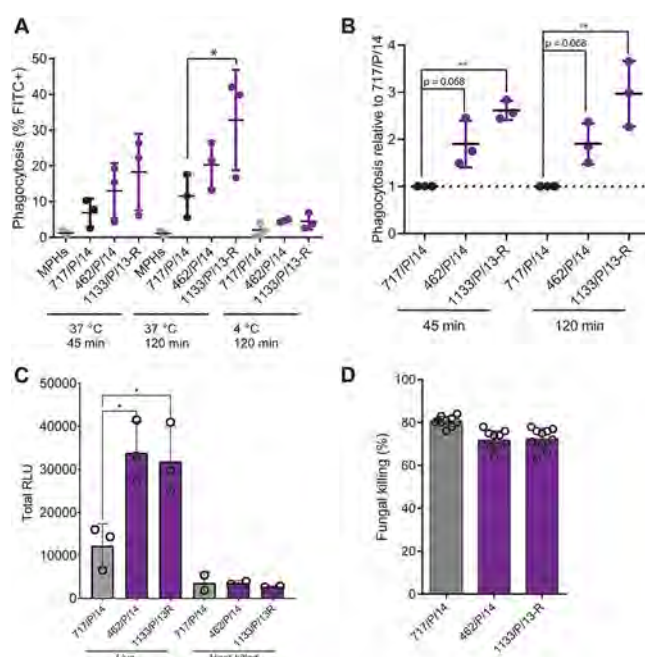


**FIG 4** ECN-R isolates undergo distinct recognition by macrophages. (A and B) Phagocytosis of FITC-labeled *C. auris* cells by bone marrow-derived macrophages (BMDMs) after 45 and 120 min of coculture as assessed by flow cytometry. Macrophages were gated according to the scheme shown in Fig. S4A in the supplemental material, and the percentages of FITC-positive (FITC<sup>+</sup>) macrophages (A) and relative phagocytosis (relative to mean 717/P/14 levels) (B) are depicted. The means (horizontal lines) and SD from biological triplicates (dots) are shown. (C) Real-time luminescence-based reactive oxygen species (ROS) assay with BMDMs cocultured with live or heat-killed (70°C for 10 min) *C. auris* cells. Relative luminescence units (RLU) were recorded every 2.5 min for at least 130 min. Representative RLU over time per 1,000 BMDMs are depicted in Fig. S4B. Data represent the mean total RLU and SD from three biological replicates measured in technical triplicates. (D) Fungal survival after 4 h of coculture with macrophages. The percentage of fungal killing represents the number of CFU recovered after BMDM interaction relative to that in *C. auris* single cultures under otherwise identical conditions. Data represent the means and SD from two independent experiments performed with five technical replicates. n.s. (not significant),  $P > 0.05$ ; \*,  $P < 0.05$ ; \*\*,  $P < 0.01$  (by one-way ANOVA followed by Tukey's multiple-comparison correction). The homoscedasticity of the data was confirmed by performing Bartlett's test. (See also Fig. S4.)

note, “clade-specific” environmental stresses coupled with anthropogenic actions may have been additional drivers (13, 59). This is reflected in the genetic and phenotypic diversities among *C. auris* clades (14). For instance, clade II isolates show a propensity for ear infections (60); they lost genes encoding putative adhesins (61) and harbor impaired stress resistance (62). Additionally, despite rather low genetic diversities within a clade (14), phenotypic intraclade variations, such as in antifungal susceptibility profiles (13, 33), cell wall structures (28), or aggregate formation (63), are known. Here, we further explored the intraclade diversity of clade I *C. auris* clinical isolates. We reveal pronounced transcriptional alterations affecting up to 24% of the *C. auris* genes detected here when ECN-S and ECN-R strains were compared. Remarkably, the deregulation of genes is reduced (2% of the detected *C. auris* genes) between independent and unrelated ECN-S clinical patient isolates. Interestingly, all tested isolates displayed FCZ resistance according to CLSI broth microdilution testing, while susceptibilities to AmB and 5-flucytosine varied among the isolates. Hence, transcriptomic alterations between these isolates may also reflect potential complex genetic compensatory mechanisms leading to distinct resistance traits that are not coupled solely to ECN-R. For instance, cell wall alterations have also been found in *Candida tropicalis* isolates resistant to AmB (64). Hence, we believe that comparing multiple ECN-R and ECN-S isolates can be helpful in limiting the detection of transcripts differentially expressed due to other isolate- or clade-specific properties. In line with this, some 362 genes were commonly differentially expressed among all three ECN-R and both ECN-S isolates. Of

note, small transcriptomic alterations also occur among isolates with divergent antifungal susceptibility profiles (33). Also of note, a recent report detected almost 1,000 differentially expressed genes between azole-resistant and -susceptible *C. auris* isolates (65). This seems surprising as clade I as well as clade III isolates of *C. auris* display the lowest intraclade genetic diversities (13). Given that the synteny and genomic arrangements are similar among the isolates investigated here, it is tempting to speculate that epigenetic factors contribute to such marked transcriptional alterations within a given clade. Thus, epigenetic signatures may be related to specific environmental stresses and pathogen “experiences” inherited by the next generation. Of note, the inheritance of stress-induced epigenetic marks is well established in mammals and plants (66). For instance, hereditary adaptive DNA methylation patterns in plants are harnessed to facilitate coevolution with new climatic conditions (67). Furthermore, the phytopathogenic fungus *Cryphonectria parasitica* shows epigenetic diversity among different haplotypes with distinctive expansion and invasion traits (68). Interestingly enough, genes mediating morphogenetic changes are enriched with heterogeneous DNA methylation patterns in *C. albicans* (69). Hence, hereditary epigenetic modifications, known as “epigenetic memory,” provide a swift adaptive-fitness advantage in response to environmental cues or host immune defenses and enable the phenotypic plasticity of clonal (sub)populations. These mechanisms are therefore considered key to the evolution of the onset and manifestation of infectious diseases (70, 71). Hence, assessing the dynamics of changing epigenetic landscapes among *C. auris* isolates coupled with transcriptional profiling is likely to yield valuable insights into the molecular and genetic mechanisms driving phenotypic diversification but also reveals the emergence of pathogenic virulence traits, including pan-antifungal resistance.

The rapid global spread and robust environmental persistence of *C. auris* as well as the increasing appearance of multi- and pan-antifungal-resistant isolates are of particular medical concern. While resistance to FCZ or AmB is frequently observed among clade I isolates, the frequency of ECN resistance remains low at the moment (11, 12, 35). As ECN stands out as the recommended first-line therapy against invasive candidiasis (72), an increase in ECN resistance among *Candida* spp. poses a serious threat to efficient antifungal therapies. Moreover, ECN resistance can develop quickly upon the onset of ECN treatment (73, 74). Mutations in *FKS* genes encoding  $\beta$ -glucan synthases are currently the major mechanisms underlying clinical ECN resistance. Drug exposure, such as with prophylactic or recurrent ECN treatment, further enhances the selection of resistance (39, 75). Of note, all of the investigated ECN-R isolates carry the *FKS1* S639F hot spot mutations, while the source patients had no history of ECN treatment. However, as *C. auris* can be transmitted from person to person by skin contact (76), the possibility remains that these isolates may originate from another patient with previous ECN exposure. Indeed, nearly clonal isolates have emerged from hospitals in north and south India (77) and can spread through local transmission (78).

Besides mutations in *FKS1*, additional regulators have been linked to increased CSP tolerance in other *Candida* spp., including *Candida glabrata* (39, 43, 74). For instance, the cell wall is intimately linked to ECN susceptibility. The genetic ablation of mannoproteins and other cell wall-related genes modulates CSP susceptibility in *C. albicans* and *C. glabrata* (43, 45). In line with this, CSP treatment readily triggers cell wall integrity signaling involving several pathways and transcription factors, thus leading to cell wall remodeling and stress adaptations (55, 79) such as increased chitin exposure (80, 81) via the activation of chitin synthesis. In line with this, *C. auris* elevates chitin levels in response to CSP treatment (82). In addition, a recent study observed elevated levels of exposed mannans in two *C. auris* isolates after 24 h of CSP exposure (55). Although the ECN-R isolates from our study did not display markedly increased chitin levels during standard laboratory growth, the mannan and  $\beta$ -glucan contents were substantially elevated in ECN-R strains. These distinct cell surface properties were further reflected in the altered adhesion potential and transcriptomic profiles of ECN-R isolates. Specifically, 16 genes annotated to the cellular component “cell wall” were commonly dysregulated in ECN-R *C. auris* isolates, with only 3 genes, *PGA6*,

*PGA31*, and *XOG1*, being upregulated. Interestingly, *PGA31* expression was upregulated in CSP-treated *C. albicans* (83), and its deletion increased CSP susceptibility (45). Additionally, *PGA6* was also upregulated in other *C. auris* isolates treated with CSP for 24 h (55). However, single-gene deletions of *PGA6* did not affect CSP susceptibility in the isolates investigated here. Moreover, the loss of *PGA6* only moderately decreased cell adhesion by the ECN-R isolates. However, the effects varied between replicates. These results imply that the combinatorial loss of dysregulated cell surface genes may be required to affect the adhesion properties of ECN-R isolates substantially. In addition, the protein kinase Gin4, which controls septin function and regulation as well as cell wall integrity (84), was found to be upregulated in all ECN-R isolates. Similarly, *PGA31* was found to be upregulated during cell wall regeneration in response to protoplasting (85). The altered expression of otherwise stress-regulated genes under basal growth conditions may reflect differential baseline levels of cellular stress and environmental sensing. Besides *FKS* mutations conferring clinical ECN resistance, other mechanisms may contribute to the accumulation of additional genomic alterations mediating ECN resistance. Indeed, ECN resistance is a multistep developmental process consisting of stress adaptations such as cell wall integrity signaling (86). In line with this, an analysis tracking genomic alterations during CSP treatment in a human host revealed the occurrence of mutations that slightly decrease CSP susceptibility prior to the development of clinical ECN resistance via *FKS* mutations in *C. glabrata* (74). As the cell wall organization was altered in all three ECN-R isolates used in this study, we speculate that these cells might have initially displayed intrinsic tolerance to ECN prior to the acquisition of the *FKS1* S639F mutation. This would favor decreased fungal clearance in response to the initial ECN treatment. This manifested tolerance would then provide a window of opportunity to further facilitate adaptive mutations that drive ECN resistance. In addition, the ECN-R isolates displayed enhanced transcription of genes involved in mitochondrial gene expression (17 core set genes out of 51 genes annotated to mitochondrial gene expression). Interestingly, mitochondrial functions were recently implicated in ECN tolerance in *C. glabrata* (40) and were also enriched transcriptionally in CSP-treated *C. auris* (55). Hence, it is tempting to speculate that the detected core set of DEGs of ECN-R isolates, such as cell surface or mitochondrial genes, reflects phenotypic adaptive responses implicated in the development of ECN tolerance and, eventually, host interactions.

Antifungal drug resistance is most likely accompanied by trade-offs in fungal fitness in certain environments such as the absence of antifungal selection pressure (74, 87, 88). Indeed, the ECN-R isolates in this study showed decreased growth rates under host interaction conditions and ameliorated fungal recognition. However, the fungal killing of ECN-R isolates by BMDMs was not enhanced after 4 h of coculture. This indicates that although initial BMDM responses are decreased upon 717/P/14 challenge, the antifungal effector mechanisms of BMDMs still exceed the threshold for efficient fungal killing after prolonged interactions. Alternatively, ECN-R isolates may be more resistant to killing by BMDMs despite increased phagocytosis and ROS stress. The differential recognition of ECN-R strains versus the ECN-S 717/P/14 isolate may result from the decreased mannan abundance of ECN-S *C. auris*. Indeed, the mannan structure of the *C. auris* cell wall is considered key in mediating innate host responses (28). As ECN-R isolates have enhanced adhesion *in vitro*, these isolates may additionally show improved adhesion to host cells, which may increase fungal survival despite putative fitness defects. Thus, future studies should address the competitive fitness of *C. auris* strains displaying distinct phenotypic traits to further elucidate the factors mediating host interactions with different *C. auris* isolates.

Taken together, we identified a set of 362 genes commonly differentially regulated in three independent ECN-R isolates compared to two unrelated ECN-S *C. auris* isolates. This core gene set is enriched in, among others, cell wall-related genes, which are well represented in the phenotypic features of these isolates, as exemplified by the altered cell wall structure, adhesion, and host immune cell interactions of ECN-R isolates. Although we investigated only a few patient isolates, this work demonstrates in

principle that phenotypic characteristics shared by distinct and unrelated patient isolates are well predictable by transcriptomic profiling. Hence, we suggest that the systematic profiling of *C. auris* transcriptomes and their integration with genomic data can facilitate the discovery of (clade-specific) transcriptional biomarkers of predictive value to assess host-fungal interactions, the propensity for antifungal resistance, and, possibly, therapeutic outcomes.

## MATERIALS AND METHODS

**Media and fungal growth conditions.** All strains used in this study are listed in Table S1 in the supplemental material. The clinical isolates of *C. auris* included 73% bloodstream isolates. The isolates were collected from the culture collection of the Medical Mycology Unit, Vallabhbhai Patel Chest Institute, University of Delhi, Delhi, India. *Candida* strains were routinely grown on YPD medium (1% yeast extract, 2% peptone, and 2% glucose [all from BD Biosciences]) at 30°C with shaking at 200 rpm. For solid medium, 2% Bacto agar (BD Biosciences) was added. Synthetic complete (SC) medium (1.7 g/L yeast nitrogen base without amino acids and ammonium sulfate [BD Biosciences], 5 g/L ammonium sulfate [Sigma-Aldrich], amino acid mix, and 2% glucose [both from BD Biosciences]) was prepared as previously described (89).

**Antifungal susceptibility screening on solid agar medium.** Antifungal susceptibility testing on solid medium was carried out essentially as described previously (33), using a robot instrument (RoToR HDA; Singer Ltd., Roadwater, UK). Briefly, *C. auris* clinical isolates were printed on YPD agar plates from cryostocks and incubated at 30°C for 3 days. Colony spots were inoculated in 200  $\mu$ L liquid YPD medium in a 96-well plate using the robot instrument and grown overnight at 30°C with constant agitation (150 rpm) prior to spotting onto solid SC medium with or without antifungal drugs using the robot instrument. Growth inhibition by antifungal treatment was assessed by the colony size after incubation for 3 days at 30°C. The colony size was calculated using the R gitter package (<https://github.com/omarwagih/gitter>) and normalized to the colony size on SC medium without an antifungal drug (equal to the relative colony size). The lower the ratio of the colony size with the drug versus no drug, the more susceptible the isolate. The following antifungals were tested: fluconazole (FCZ; Discovery Fine Chemicals Ltd.) (64  $\mu$ g/mL in dimethyl sulfoxide [DMSO] [Sigma-Aldrich]), itraconazole (ICZ; Discovery Fine Chemicals Ltd.) (0.15  $\mu$ g/mL in DMSO), voriconazole (VCZ; Discovery Fine Chemicals Ltd.) (0.15  $\mu$ g/mL in DMSO), amphotericin B (AmB; Santa Cruz Biotechnology) (3.0  $\mu$ g/mL in DMSO), caspofungin (CSP; Merck) (0.40  $\mu$ g/mL in distilled water [dH<sub>2</sub>O]), and 5-fluorocytosine (5-FC; Sigma-Aldrich) (10  $\mu$ g/mL in dH<sub>2</sub>O).

**Growth inhibition assays.** Growth inhibition of *C. auris* isolates by antifungals, calcofluor white (Sigma-Aldrich), and antimycin A (Sigma-Aldrich) was assessed using an MIC assay in liquid YPD medium exactly as described previously (33). Optical density at 600 nm (OD<sub>600</sub>) readings were performed after 24 h of incubation at 30°C using a Victor Nivo plate reader (PerkinElmer). The percentage of growth represents the OD<sub>600</sub> values in response to drug treatment relative to the OD<sub>600</sub> readings of strains grown in YPD medium only. For drugs dissolved in DMSO, the corresponding DMSO concentration (2% final concentration) was included for untreated samples. In addition, MIC values of antifungals against *C. auris* isolates were assessed based on guidelines of Clinical and Laboratory Standards Institute (CLSI) M27-A3 protocols (90).

**Generation of gene deletion mutants.** *C. auris* gene deletion mutants were constructed using a fusion PCR strategy exactly as described previously (43). Briefly, roughly 500-bp flanking regions upstream and downstream of the *C. auris* target gene were amplified from genomic DNA (gDNA) extracted from the CBS10913 strain as described previously (33). The *NAT1* selection marker was amplified from the plasmid pTS50 (43). The PCR-amplified flanking regions and the *NAT1* selection marker were purified on a 1% agarose gel (PeqLab) and extracted using the GeneJET gel extraction kit (Thermo Scientific). Purified PCR products then served as the template for the fusion PCR to generate the final gene deletion cassette. The transformation of *C. auris* with the gene deletion cassette was carried out as reported previously (91). The correct genomic integration of the deletion construct and the loss of the target gene were verified by colony PCR (92). The oligonucleotides used in this study are listed in Table S2.

**Transcriptional profiling using RNA sequencing.** For RNA sequencing (RNA-seq) analysis, *C. auris* cultures grown overnight were inoculated into YPD medium (initial OD<sub>600</sub> of 0.1) and grown at 30°C for 4 h. Total RNA was purified using a GeneJET RNA purification kit (Thermo Scientific). The quality of RNA was assessed on a Bioanalyzer using the RNA6000 Nano chip (Agilent), mRNA was enriched using oligo (dT) beads (New England BioLabs [NEB]), and subsequently, double-stranded cDNA libraries were generated by using the NEBNext Ultra directional RNA library prep kit for Illumina (NEB) according to the manufacturer's instructions. The qualified libraries were subjected to Illumina sequencing with 150-bp paired-end reads at the Novogene sequencing facility. Three biological replicates for each strain were sequenced.

Quality control of raw sequencing reads was done using fastQC v0.11.8 (93). TrueSeq (Illumina) adapters were trimmed using cutadapt v1.18 (<https://cutadapt.readthedocs.io/en/stable/>) (settings –interleaved –q 30), followed by read mapping onto the *C. auris* B8441 genome assembly (*Candida* Genome Database version s01-m01-r10 [<http://www.candidagenome.org/>]) using NextGenMap v0.5.5 (94) (settings -b -Q 30). Optical read duplicates were removed using Picard tools (Broad Institute [<https://broadinstitute.github.io/picard/>]) (settings MarkDuplicates REMOVE\_SEQUENCING\_DUPLICATES=true). Read counting was done using HTseq (95) in the union mode and the genomic annotation from *C. auris* B8841 (settings -f bam -r pos -t gene -i ID), and read coverage profiles were visualized using the Integrative Genomics Viewer (IGV) (96). Differential gene



expression analysis was done using pairwise comparisons in edgeR (97). The false discovery rate (FDRs) represent *P* values adjusted for multiple testing using the Benjamini-Hochberg procedure (98). Normalized read counts were extracted using the edgeR cpm function and were used for principal-component analysis (PCA) using the prcomp function in R.

GO term enrichment analysis based on the *C. albicans* homologues was performed using the enrichGO function from the clusterProfiler package (99). Only GO categories with a *q* value of <0.05 were considered significant. Gene set enrichment analysis was done using the clusterProfiler gseGO function. *C. albicans* homologues were retrieved from the *Candida* Genome Database (<http://www.candidagenome.org/>). Venn diagrams were generated using the VennDiagram package in R (100). The RNA-seq analysis results are summarized in Table S3, all GO enrichment results are shown in Table S4, and data used to generate the heatmaps are shown in Table S5.

**Plastic adhesion assay.** *C. auris* isolates were grown to the logarithmic phase in YPD medium at 30°C and counted on a CASY counter (Roche). Cells were then diluted to  $1 \times 10^6$  cells/mL in YPD medium, and aliquots of 100  $\mu$ L of this dilution were distributed into a well of a 96-well polystyrene plate (tissue culture treated; CytoOne). The plate was then incubated in a static incubator at 37°C for 4 h, and the adhered fungal biomass was subsequently quantified using crystal violet. Briefly, YPD medium was removed by inverting the plate and tapping it on paper towels. The wells were then washed three times with phosphate-buffered saline (PBS) and incubated with 100  $\mu$ L methanol (Merck) for 15 min. The plates were left to dry overnight in a chemical safety cabinet, followed by staining with 100  $\mu$ L 0.1% crystal violet for 5 min and three washes with  $\text{dH}_2\text{O}$ . Crystal violet was dissolved from the stained biomass by adding 100  $\mu$ L of 33% acetic acid and by plate shaking for 1 min at 800 rpm. The supernatants of dissolved crystal violet were transferred into fresh wells of a 96-well plate, and the absorbance at 590 nm was recorded using a Victor Nivo plate reader (PerkinElmer).

**Quantification of cell wall components.** Chitin, mannans, and exposed  $\beta$ -glucans were simultaneously quantified from *C. auris* isolates using flow cytometry as described previously, with modifications (101). Briefly, cells were precultured in YPD medium at 30°C with constant agitation for 4 to 5 h, followed by OD<sub>600</sub> measurement. An aliquot of the preculture was then inoculated into fresh YPD medium to retrieve a culture at an OD<sub>600</sub> of 1 to 2 after 15 to 17 h of further incubation at 30°C with constant agitation. The cells were then counted on a CASY counter (Roche), and  $2 \times 10^6$  cells were washed 3 times with fluorescence-activated cell sorter (FACS) buffer (1% fetal calf serum [FCS; Gibco], 0.5 mM EDTA, and 0.1% Tween 20 [both from Sigma-Aldrich] in PBS). To stain exposed  $\beta$ -glucans, cells were incubated with 5 ng/mL of Fc (human)-dectin-1 (AdipoGen) in FACS buffer on ice for 60 min. The cells were washed 3 times with FACS buffer and subsequently incubated with a 2.5- $\mu$ g/mL final concentration of Alexa Fluor 488 anti-human IgG Fc antibody (BioLegend) on ice for 45 min, followed by 3 washes with FACS buffer and mannan staining using a 25- $\mu$ g/mL final concentration of concanavalin A-Texas Red (Thermo Fisher) in FACS buffer at 30°C for 45 min. The cells were then washed again 3 times with FACS buffer, and chitin was stained with a 25- $\mu$ g/mL final concentration of calcofluor white (Sigma-Aldrich) in FACS buffer. Samples were measured on an LSRFortessa cytometer (BD Biosciences), including unstained and singly stained controls.

The total  $\beta$ -glucan levels were assessed using a slightly modified aniline blue staining protocol described previously (102). Briefly, cells were grown as described above, put on ice, and washed twice with ice-cold PBS. Cells were then counted, diluted to  $1 \times 10^6$  cells/mL in a solution containing 1 M glycine (pH 9.5) and 0.005% aniline blue, and stained for 5 min. Unstained cells incubated for 5 min in 1 M glycine (pH 9.5) were included as controls. Samples were then subsequently measured on an LSRFortessa instrument (BD Biosciences).

Raw flow cytometry data were analyzed with FlowJo v7 (FlowJo software version 7.6.5), and the gating strategy is displayed in Fig. S3D.

**Coculture assays with primary macrophages.** Bone marrow-derived macrophages (BMDMs) were differentiated from the bone marrow of C57BL/6J mice essentially as described previously (103). For BMDM-*C. auris* cocultures, *C. auris* cells were cultured in YPD medium at 30°C with constant agitation to the logarithmic growth phase, washed 3 times with PBS, and counted on a CASY cell counter (Roche).

Fungal killing by BMDMs was analyzed as previously described (104). Briefly,  $1 \times 10^5$  BMDMs were seeded into a well of a 96-well plate (tissue culture treated; Starlab) 1 day prior to the assay. The next day, BMDMs were infected with 50  $\mu$ L PBS containing  $1 \times 10^4$  *C. auris* cells, resulting in a multiplicity of infection (MOI) of 1:10 (fungi/BMDMs), and incubated for 4 h at 37°C with 5% CO<sub>2</sub>. Fungal cells were collected after the addition of 50  $\mu$ L 4% SDS-PBS and well scraping with plastic tips. The contents of the scraped wells were transferred into 400  $\mu$ L PBS, which were pooled with two PBS washes (200  $\mu$ L per wash). Dilutions of the collected cells were plated onto YPD plates, and CFU were quantified after 48 h at 30°C. *C. auris* cells without BMDMs were cultured under otherwise identical conditions as the input control. The percentage of fungal killing represents the ratio of recovered CFU from *C. auris* cells cultured with BMDMs to CFU from *C. auris* single cultures (input control).

Phagocytosis assays with BMDMs were carried out as reported previously (105), with modifications. *C. auris* isolates were stained with 1 mg/mL FITC (Sigma-Aldrich) for 30 min at 30°C and washed 3 times with PBS prior to BMDM ( $2 \times 10^5$  to  $3 \times 10^5$  BMDMs per well of a 24-well plate [Starlab]) infection at an MOI of 2:1 (fungi/BMDMs) for 45 and 120 min at 37°C with 5% CO<sub>2</sub>. In parallel, a BMDM-*C. auris* coculture was kept at 4°C as a negative control. After the incubation time, the plates were immediately put on ice, and BMDMs were washed 3 times with cold PBS. Extracellular FITC fluorescence was quenched with 200  $\mu$ L 0.4% trypan blue (Sigma-Aldrich) for 15 min at 4°C, followed by 3 washes with cold PBS. BMDMs were then treated with 250  $\mu$ L trypsin (Sigma-Aldrich) for 5 min at 37°C and harvested in 750  $\mu$ L Dulbecco's modified Eagle's medium (DMEM)–10% heat-inactivated FCS (hiFCS) by pipetting. BMDMs were pelleted at  $300 \times g$  at 4°C for 4 min and resuspended in 300  $\mu$ L FACS buffer (PBS plus 0.1% bovine

serum albumin [BSA] [both from Sigma-Aldrich]). Samples were measured on an LSRFortessa cytometer (BD Biosciences), including BMDMs without FITC-labeled *C. auris* and *C. auris* singly stained controls. Raw flow cytometry data were analyzed with FlowJo v7 (FlowJo software version 7.6.5).

Reactive oxygen species (ROS) responses in BMDMs cocultured with *C. auris* were assessed using a luminol-based assay essentially as described previously (106). Briefly,  $4 \times 10^4$  BMDMs were seeded into a well of a 96-well plate (tissue culture treated, white walled; Thermo Scientific) the day prior to the assays. BMDMs were then washed twice with prewarmed PBS, followed by the addition of 100  $\mu$ L prewarmed Hanks' balanced salt solution (HBSS) with  $Mg^{2+}$  and  $Ca^{2+}$  (Gibco). *C. auris* cells were resuspended in HBSS with  $Mg^{2+}$  and  $Ca^{2+}$  and adjusted to  $4 \times 10^6$  fungal cells per mL. Luminol and horseradish peroxidase (HRP) type VI (both from Sigma) were diluted in HBSS with  $Mg^{2+}$  and  $Ca^{2+}$  to final concentrations of 200  $\mu$ M and 16 U, respectively, and 50  $\mu$ L of this mix was added to the BMDMs, followed by the addition of 50  $\mu$ L of the adjusted *C. auris* cell suspension, resulting in an MOI of 5:1 (fungi/BMDMs). Chemiluminescence was recorded in real time at 2.5-min intervals at 30°C using a Victor Nivo plate reader (PerkinElmer). Raw relative luciferase units (RLU) were blanked with values from BMDM single cultures and are presented as RLU per minute over time or as total RLU for the indicated time span.

**Fungal growth in BMDM medium.** *C. auris* cells were grown in YPD medium overnight at 30°C with constant agitation. Cultures were washed twice in  $dH_2O$  prior to reinoculation into BMDM medium (L-conditioned DMEM [high glucose without pyruvate] and 10% heat-inactivated FCS) "to" (DMEM [high glucose without pyruvate] containing 15% L929-conditioned cell supernatant and 10% heat-inactivated FCS [L-conditioned DMEM]).

**Statistical analysis.** Statistical significance was assessed using GraphPad Prism 9 (GraphPad Software, Inc.) or RStudio (107). The number of biological replicates is stated in each figure legend. Error bars represent the standard deviations (SD) of the means. Unless otherwise stated, two-sample comparisons were analyzed using unpaired two-sided Student's *t* tests. Multigroup comparisons were assessed using one-way analysis of variance (ANOVA) with Tukey's multiple-comparison correction.  $IC_{50}$  values were calculated using nonlinear regression (four-parameter dose-response curve) in GraphPad Prism 9 (GraphPad Software, Inc.) (\*,  $P < 0.05$ ; \*\*,  $P < 0.01$ ; \*\*\*,  $P < 0.001$ ; ns, not statistically significant).

**Data availability.** RNA-seq data sets have been deposited at the Gene Expression Omnibus (GEO) (accession number [GSE198410](https://www.ncbi.nlm.nih.gov/geo/query/acc.cgi?acc=GSE198410)). Scripts used for the primary RNA-seq bioinformatics workflow are freely available on GitHub ([https://github.com/tschemic/RNAseq\\_analysis\\_Cauris](https://github.com/tschemic/RNAseq_analysis_Cauris)).

## SUPPLEMENTAL MATERIAL

Supplemental material is available online only.

**FIG S1**, TIF file, 2.1 MB.

**FIG S2**, TIF file, 2.5 MB.

**FIG S3**, TIF file, 2.3 MB.

**FIG S4**, TIF file, 1.8 MB.

**TABLE S1**, PDF file, 0.3 MB.

**TABLE S2**, PDF file, 0.2 MB.

**TABLE S3**, XLSX file, 1.5 MB.

**TABLE S4**, XLSX file, 0.03 MB.

**TABLE S5**, XLSX file, 0.03 MB.

## ACKNOWLEDGMENTS

This work was funded by a grant from the Austrian Science Fund (FWF) (ChromFunVir) (P-32582) to K.K. In addition, support came in part from a grant from the National Institutes of Health to N.C. and K.K. (R01AI124499). P.C.T. was supported by a student fellowship from the Ernst Mach Grant-ASEA-UNINET through the Austrian Academic Exchange (OeAD). I.T. was supported through the doc.funds doctoral program TissueHome funded by the FWF, and P.P. was supported by the special research area grant SFB-F70-HIT from the FWF.

## REFERENCES

- Gudipati S, Zervos M, Herc E. 2020. Can the One Health approach save us from the emergence and reemergence of infectious pathogens in the era of climate change: implications for antimicrobial resistance? *Antibiotics* (Basel) 9:599. <https://doi.org/10.3390/antibiotics9090599>.
- The Lancet Microbe. 2021. Climate change: fires, floods, and infectious diseases. *Lancet Microbe* 2:e415. [https://doi.org/10.1016/S2666-5247\(21\)00220-2](https://doi.org/10.1016/S2666-5247(21)00220-2).
- Jackson BR, Chow N, Forsberg K, Litvinseva AP, Lockhart SR, Welsh R, Vallabhaneni S, Chiller T. 2019. On the origins of a species: what might explain the rise of *Candida auris*? *J Fungi* (Basel) 5:58. <https://doi.org/10.3390/jof5030058>.
- Ventola CL. 2015. The antibiotic resistance crisis. Part 1: causes and threats. *PT* 40:277–283.
- Levy SB, Marshall B. 2004. Antibacterial resistance worldwide: causes, challenges and responses. *Nat Med* 10:S122–S129. <https://doi.org/10.1038/nm1145>.
- Casadevall A, Kontoyiannis DP, Robert V. 2019. On the emergence of *Candida auris*: climate change, azoles, swamps, and birds. *mBio* 10:e01397-19. <https://doi.org/10.1128/mBio.01397-19>.
- Arora P, Singh P, Wang Y, Yadav A, Pawar K, Singh A, Padmavati G, Xu J, Chowdhary A. 2021. Environmental isolation of *Candida auris* from the

- coastal wetlands of Andaman Islands, India. *mBio* 12:e03181-20. <https://doi.org/10.1128/mBio.03181-20>.
8. Satoh K, Makimura K, Hasumi Y, Nishiyama Y, Uchida K, Yamaguchi H. 2009. *Candida auris* sp. nov., a novel ascomycetous yeast isolated from the external ear canal of an inpatient in a Japanese hospital. *Microbiol Immunol* 53:41–44. <https://doi.org/10.1111/j.1348-0421.2008.00083.x>.
  9. Meis JF, Chowdhary A. 2018. *Candida auris*: a global fungal public health threat. *Lancet Infect Dis* 18:1298–1299. [https://doi.org/10.1016/S1473-3099\(18\)30609-1](https://doi.org/10.1016/S1473-3099(18)30609-1).
  10. Chakrabarti A, Sood P. 2021. On the emergence, spread and resistance of *Candida auris*: host, pathogen and environmental tipping points. *J Med Microbiol* 70:001318. <https://doi.org/10.1099/jmm.0.001318>.
  11. Lockhart SR, Etienne KA, Vallabhaneni S, Farooqi J, Chowdhary A, Govender NP, Colombo AL, Calvo B, Cuomo CA, Desjardins CA, Berkow EL, Castanheira M, Magobo RE, Jabeen K, Asghar RJ, Meis JF, Jackson B, Chiller T, Litvintseva AP. 2017. Simultaneous emergence of multidrug-resistant *Candida auris* on 3 continents confirmed by whole-genome sequencing and epidemiological analyses. *Clin Infect Dis* 64:134–140. <https://doi.org/10.1093/cid/ciw691>.
  12. Chowdhary A, Prakash A, Sharma C, Kordalewska M, Kumar A, Sarma S, Tarai B, Singh A, Upadhyaya G, Upadhyay S, Yadav P, Singh PK, Khillan V, Sachdeva N, Perlin DS, Meis JF. 2018. A multicentre study of antifungal susceptibility patterns among 350 *Candida auris* isolates (2009–17) in India: role of the *ERG11* and *FKS1* genes in azole and echinocandin resistance. *J Antimicrob Chemother* 73:891–899. <https://doi.org/10.1093/jac/dkx480>.
  13. Chow NA, Muñoz JF, Gade L, Berkow EL, Li X, Welsh RM, Forsberg K, Lockhart SR, Adam R, Alanio A, Alastruey-Izquierdo A, Althawadi S, Araúz AB, Ben-Ami R, Bharat A, Calvo B, Desnos-Ollivier M, Escandón P, Gardam D, Gunturu R, Heath CH, Kurzai O, Martin R, Litvintseva AP, Cuomo CA. 2020. Tracing the evolutionary history and global expansion of *Candida auris* using population genomic analyses. *mBio* 11:e03364-19. <https://doi.org/10.1128/mBio.03364-19>.
  14. Muñoz JF, Gade L, Chow NA, Loparev VN, Juieng P, Berkow EL, Farrer RA, Litvintseva AP, Cuomo CA. 2018. Genomic insights into multidrug-resistance, mating and virulence in *Candida auris* and related emerging species. *Nat Commun* 9:5346. <https://doi.org/10.1038/s41467-018-07779-6>.
  15. Chen J, Tian S, Han X, Chu Y, Wang Q, Zhou B, Shang H. 2020. Is the superbug fungus really so scary? A systematic review and meta-analysis of global epidemiology and mortality of *Candida auris*. *BMC Infect Dis* 20:827. <https://doi.org/10.1186/s12879-020-05543-0>.
  16. Lockhart SR. 2019. *Candida auris* and multidrug resistance: defining the new normal. *Fungal Genet Biol* 131:103243. <https://doi.org/10.1016/j.fgb.2019.103243>.
  17. Berman J, Krysan DJ. 2020. Drug resistance and tolerance in fungi. *Nat Rev Microbiol* 18:319–331. <https://doi.org/10.1038/s41579-019-0322-2>.
  18. Centers for Disease Control and Prevention. 2019. Antibiotic resistance threats in the United States. Centers for Disease Control and Prevention, Atlanta GA.
  19. Carolus H, Jacobs S, Lobo Romero C, Deparis Q, Cuomo CA, Meis JF, Van Dijk P. 2021. Diagnostic allele-specific PCR for the identification of *Candida auris* clades. *J Fungi (Basel)* 7:754. <https://doi.org/10.3390/jof7090754>.
  20. Forsberg K, Woodworth K, Walters M, Berkow EL, Jackson B, Chiller T, Vallabhaneni S. 2019. *Candida auris*: the recent emergence of a multi-drug-resistant fungal pathogen. *Med Mycol* 57:1–12. <https://doi.org/10.1093/mmy/myy054>.
  21. Briard B, Fontaine T, Kanneganti T-D, Gow NAR, Papon N. 2021. Fungal cell wall components modulate our immune system. *Cell Surf* 7:100067. <https://doi.org/10.1016/j.tcsu.2021.100067>.
  22. Hall RA, Gow NAR. 2013. Mannosylation in *Candida albicans*: role in cell wall function and immune recognition. *Mol Microbiol* 90:1147–1161. <https://doi.org/10.1111/mmi.12426>.
  23. Hopke A, Brown AJP, Hall RA, Wheeler RT. 2018. Dynamic fungal cell wall architecture in stress adaptation and immune evasion. *Trends Microbiol* 26:284–295. <https://doi.org/10.1016/j.tim.2018.01.007>.
  24. Garcia-Effron G, Lee S, Park S, Cleary JD, Perlin DS. 2009. Effect of *Candida glabrata* *FKS1* and *FKS2* mutations on echinocandin sensitivity and kinetics of 1,3- $\beta$ -D-glucan synthase: implication for the existing susceptibility breakpoint. *Antimicrob Agents Chemother* 53:3690–3699. <https://doi.org/10.1128/AAC.00443-09>.
  25. Park S, Kelly R, Kahn JN, Robles J, Hsu M-J, Register E, Li W, Vyas V, Fan H, Abruzzo G, Flattery A, Gill C, Chrebet G, Parent SA, Kurtz M, Teppler H, Douglas CM, Perlin DS. 2005. Specific substitutions in the echinocandin target Fks1p account for reduced susceptibility of rare laboratory and clinical *Candida* sp. isolates. *Antimicrob Agents Chemother* 49:3264–3273. <https://doi.org/10.1128/AAC.49.8.3264-3273.2005>.
  26. Gow NAR, Hube B. 2012. Importance of the *Candida albicans* cell wall during commensalism and infection. *Curr Opin Microbiol* 15:406–412. <https://doi.org/10.1016/j.mib.2012.04.005>.
  27. Netea MG, Joosten LAB, Van Der Meer JWM, Kullberg BJ, Van De Veerdonk FL. 2015. Immune defence against *Candida* fungal infections. *Nat Rev Immunol* 15:630–642. <https://doi.org/10.1038/nri3897>.
  28. Bruno M, Kersten S, Bain JM, Jaeger M, Rosati D, Kruppa MD, Lowman DW, Rice PJ, Graves B, Ma Z, Jiao YN, Chowdhary A, Renieris G, van de Veerdonk FL, Kullberg B-J, Giamarellos-Bourboulis EJ, Hoischen A, Gow NAR, Brown AJP, Meis JF, Williams DL, Netea MG. 2020. Transcriptional and functional insights into the host immune response against the emerging fungal pathogen *Candida auris*. *Nat Microbiol* 5:1516–1531. <https://doi.org/10.1038/s41564-020-0780-3>.
  29. Huang X, Hurabielle C, Drummond RA, Bouladoux N, Desai JV, Sim CK, Belkaid Y, Lionakis MS, Segre JA. 2021. Murine model of colonization with fungal pathogen *Candida auris* to explore skin tropism, host risk factors and therapeutic strategies. *Cell Host Microbe* 29:210–221.e6. <https://doi.org/10.1016/j.chom.2020.12.002>.
  30. Brown JL, Delaney C, Short B, Butcher MC, McCloud E, Williams C, Kean R, Ramage G. 2020. *Candida auris* phenotypic heterogeneity determines pathogenicity in vitro. *mSphere* 5:e00371-20. <https://doi.org/10.1128/mSphere.00371-20>.
  31. Zamith-Miranda D, Heyman HM, Cleare LG, Couvillion SP, Clair GC, Bredeweg EL, Gacser A, Nimrichter L, Nakayasu ES, Nosanchuk JD. 2019. Multi-omics signature of *Candida auris*, an emerging and multidrug-resistant pathogen. *mSystems* 4:e00257-19. <https://doi.org/10.1128/mSystems.00257-19>.
  32. Zamith-Miranda D, Heyman HM, Couvillion SP, Cordero RJB, Rodrigues ML, Nimrichter L, Casadevall A, Amatuzei RF, Alves LR, Nakayasu ES, Nosanchuk JD. 2021. Comparative molecular and immunoregulatory analysis of extracellular vesicles from *Candida albicans* and *Candida auris*. *mSystems* 6:e00822-21. <https://doi.org/10.1128/mSystems.00822-21>.
  33. Jenull S, Tscherner M, Kashko N, Shivarathri R, Stoiber A, Chauhan M, Petryshyn A, Chauhan N, Kuchler K. 2021. Transcriptome signatures predict phenotypic variations of *Candida auris*. *Front Cell Infect Microbiol* 11:662563. <https://doi.org/10.3389/fcimb.2021.662563>.
  34. Public Health England. 2017. Guidance for the laboratory investigation, management and infection prevention and control for cases of *Candida auris*. Public Health England, London, United Kingdom.
  35. Du H, Bing J, Hu T, Ennis CL, Noble CJ, Huang G. 2020. *Candida auris*: epidemiology, biology, antifungal resistance, and virulence. *PLoS Pathog* 16:e1008921. <https://doi.org/10.1371/journal.ppat.1008921>.
  36. Kordalewska M, Lee A, Park S, Berrio I, Chowdhary A, Zhao Y, Perlin DS. 2018. Understanding echinocandin resistance in the emerging pathogen *Candida auris*. *Antimicrob Agents Chemother* 62:e00238-18. <https://doi.org/10.1128/AAC.00238-18>.
  37. Centers for Disease Control and Prevention. 2017. Recommendations for identification of *Candida auris*. Centers for Disease Control and Prevention, Atlanta, GA.
  38. Duvenage L, Munro CA, Gourlay CW. 2019. The potential of respiration inhibition as a new approach to combat human fungal pathogens. *Curr Genet* 65:1347–1353. <https://doi.org/10.1007/s00294-019-01001-w>.
  39. Yang F, Zhang L, Wakabayashi H, Myers J, Jiang Y, Cao Y, Jimenez-Ortigosa C, Perlin DS, Rustchenko E. 2017. Tolerance to caspofungin in *Candida albicans* is associated with at least three distinctive mechanisms that govern expression of *FKS* genes and cell wall remodeling. *Antimicrob Agents Chemother* 61:e00071-17. <https://doi.org/10.1128/AAC.00071-17>.
  40. Garcia-Rubio R, Hernandez RY, Clear A, Healey KR, Shor E, Perlin DS. 2021. Critical assessment of cell wall integrity factors contributing to in vivo echinocandin tolerance and resistance in *Candida glabrata*. *Front Microbiol* 12:702779. <https://doi.org/10.3389/fmicb.2021.702779>.
  41. Perlin DS, Rautemaa-Richardson R, Alastruey-Izquierdo A. 2017. The global problem of antifungal resistance: prevalence, mechanisms, and management. *Lancet Infect Dis* 17:e383–e392. [https://doi.org/10.1016/S1473-3099\(17\)30316-X](https://doi.org/10.1016/S1473-3099(17)30316-X).
  42. Caplan T, Polvi EJ, Xie JL, Buckhalter S, Leach MD, Robbins N, Cowen LE. 2018. Functional genomic screening reveals core modulators of echinocandin stress responses in *Candida albicans*. *Cell Rep* 23:2292–2298. <https://doi.org/10.1016/j.celrep.2018.04.084>.
  43. Schwarzmüller T, Ma B, Hiller E, Istel F, Tscherner M, Brunke S, Ames L, Firon A, Green B, Cabral V, Marcet-Houben M, Jacobsen ID, Quintin J, Seider K, Frohner I, Glaser W, Jungwirth H, Bachellier-Bassi S, Chauvel M, Zeidler U, Ferrandon D, Gabaldón T, Hube B, d'Enfert C, Rupp S, Cormack B, Haynes K,



- Kuchler K. 2014. Systematic phenotyping of a large-scale *Candida glabrata* deletion collection reveals novel antifungal tolerance genes. *PLoS Pathog* 10:e1004211. <https://doi.org/10.1371/journal.ppat.1004211>.
44. Heredia MY, Gunasekaran D, Ikeh MAC, Nobile CJ, Rauceo JM. 2020. Transcriptional regulation of the caspofungin-induced cell wall damage response in *Candida albicans*. *Curr Genet* 66:1059–1068. <https://doi.org/10.1007/s00294-020-01105-8>.
  45. Plaine A, Walker L, Da Costa G, Mora-Montes HM, McKinnon A, Gow NAR, Gaillardin C, Munro CA, Richard ML. 2008. Functional analysis of *Candida albicans* GPI-anchored proteins: roles in cell wall integrity and caspofungin sensitivity. *Fungal Genet Biol* 45:1404–1414. <https://doi.org/10.1016/j.fgb.2008.08.003>.
  46. Del Mar González M, Díez-Orejas R, Molero G, Álvarez AM, Pla J, Pla J, Nombela C, Sánchez-Pérez M. 1997. Phenotypic characterization of a *Candida albicans* strain deficient in its major exoglucanase. *Microbiology (Reading)* 143:3023–3032. <https://doi.org/10.1099/00221287-143-9-3023>.
  47. Yang M, Solis NV, Marshall M, Garleb R, Zhou T, Wang D, Swidergall M, Pearlman E, Filler SG, Liu H. 2022. Control of  $\beta$ -glucan exposure by the endo-1,3-glucanase Eng1 in *Candida albicans* modulates virulence. *PLoS Pathog* 18:e1010192. <https://doi.org/10.1371/journal.ppat.1010192>.
  48. Kempf M, Cottin J, Licznar P, Lefrançois C, Robert R, Apaire-Marchais V. 2009. Disruption of the GPI protein-encoding gene *IFF4* of *Candida albicans* results in decreased adherence and virulence. *Mycopathologia* 168:73–77. <https://doi.org/10.1007/s11046-009-9201-0>.
  49. de Groot PWJ, Hellingwerf KJ, Klis FM. 2003. Genome-wide identification of fungal GPI proteins. *Yeast* 20:781–796. <https://doi.org/10.1002/yea.1007>.
  50. Liu Y, Filler SG. 2011. *Candida albicans* Als3, a multifunctional adhesin and invasin. *Eukaryot Cell* 10:168–173. <https://doi.org/10.1128/EC.00279-10>.
  51. Hall RA. 2015. Dressed to impress: impact of environmental adaptation on the *Candida albicans* cell wall. *Mol Microbiol* 97:7–17. <https://doi.org/10.1111/mmi.13020>.
  52. Bates S, MacCallum DM, Bertram G, Munro CA, Hughes HB, Buurman ET, Brown AJP, Odds FC, Gow NAR. 2005. *Candida albicans* Pmr1p, a secretory pathway P-type  $\text{Ca}^{2+}/\text{Mn}^{2+}$ -ATPase, is required for glycosylation and virulence. *J Biol Chem* 280:23408–23415. <https://doi.org/10.1074/jbc.M502162200>.
  53. Hall RA, Bates S, Lenardon MD, MacCallum DM, Wagener J, Lowman DW, Kruppa MD, Williams DL, Odds FC, Brown AJP, Gow NAR. 2013. The Mnn2 mannosyltransferase family modulates mannoprotein fibril length, immune recognition and virulence of *Candida albicans*. *PLoS Pathog* 9:e1003276. <https://doi.org/10.1371/journal.ppat.1003276>.
  54. Cabral V, Znaidi S, Walker LA, Martin-Yken H, Dague E, Legrand M, Lee K, Chauvel M, Firon A, Rossignol T, Richard ML, Munro CA, Bachellier-Bassi S, d'Enfert C. 2014. Targeted changes of the cell wall proteome influence *Candida albicans* ability to form single- and multi-strain biofilms. *PLoS Pathog* 10:e1004542. <https://doi.org/10.1371/journal.ppat.1004542>.
  55. Zamith-Miranda D, Amatuzzi RF, Munhoz da Rocha IF, Martins ST, Lucena ACR, Vieira AZ, Trentin G, Almeida F, Rodrigues ML, Nakayasu ES, Nosanchuk JD, Alves LR. 2021. Transcriptional and translational landscape of *Candida auris* in response to caspofungin. *Comput Struct Biotechnol J* 19:5264–5277. <https://doi.org/10.1016/j.csbj.2021.09.007>.
  56. Brown AJP, Budge S, Kaloriti D, Tillmann A, Jacobsen MD, Yin Z, Ene IV, Bohovych I, Sandai D, Kastora S, Potrykus J, Ballou ER, Childers DS, Shahana S, Leach MD. 2014. Stress adaptation in a pathogenic fungus. *J Exp Biol* 217:144–155. <https://doi.org/10.1242/jeb.088930>.
  57. Billmyre RB, Heitman J. 2017. Genetic and epigenetic engines of diversity in pathogenic microbes. *PLoS Pathog* 13:e1006468. <https://doi.org/10.1371/journal.ppat.1006468>.
  58. Chybowska AD, Childers DS, Farrer RA. 2020. Nine things genomics can tell us about *Candida auris*. *Front Genet* 11:351. <https://doi.org/10.3389/fgene.2020.00351>.
  59. Sharma M, Chakrabarti A. 2020. On the origin of *Candida auris*: ancestor, environmental stresses, and antiseptics. *mBio* 11:e02102-20. <https://doi.org/10.1128/mBio.02102-20>.
  60. Kwon YJ, Shin JH, Byun SA, Choi MJ, Won EJ, Lee D, Lee SY, Chun S, Lee JH, Choi HJ, Kee SJ, Kim SH, Shin MG. 2019. *Candida auris* clinical isolates from South Korea: identification, antifungal susceptibility, and genotyping. *J Clin Microbiol* 57:e01624-18. <https://doi.org/10.1128/JCM.01624-18>.
  61. Muñoz JF, Welsh RM, Shea T, Batra D, Gade L, Howard D, Rowe LA, Meis JF, Litvintseva AP, Cuomo CA. 2021. Clade-specific chromosomal rearrangements and loss of subtelomeric adhesins in *Candida auris*. *Genetics* 218:iyab029. <https://doi.org/10.1093/genetics/iyab029>.
  62. Heaney H, Laing J, Paterson L, Walker AW, Gow NAR, Johnson EM, MacCallum DM, Brown AJP. 2020. The environmental stress sensitivities of pathogenic *Candida* species, including *Candida auris*, and implications for their spread in the hospital setting. *Med Mycol* 58:744–755. <https://doi.org/10.1093/mmy/myz2127>.
  63. Szekeley A, Borman AM, Johnson EM. 2019. *Candida auris* isolates of the Southern Asian and South African lineages exhibit different phenotypic and antifungal susceptibility profiles *in vitro*. *J Clin Microbiol* 57:e02055-18. <https://doi.org/10.1128/JCM.02055-18>.
  64. Mesa-Arango AC, Rueda C, Román E, Quintin J, Terrón MC, Luque D, Netea MG, Pla J, Zaragoza O. 2016. Cell wall changes in amphotericin B-resistant strains from *Candida tropicalis* and relationship with the immune responses elicited by the host. *Antimicrob Agents Chemother* 60:2326–2335. <https://doi.org/10.1128/AAC.02681-15>.
  65. Zhou W, Li X, Lin Y, Yan W, Jiang S, Huang X, Yang X, Qiao D, Li N. 2021. A comparative transcriptome between anti-drug sensitive and resistant *Candida auris* in China. *Front Microbiol* 12:708009. <https://doi.org/10.3389/fmicb.2021.708009>.
  66. Miska EA, Ferguson-Smith AC. 2016. Transgenerational inheritance: models and mechanisms of non-DNA sequence-based inheritance. *Science* 354:59–63. <https://doi.org/10.1126/science.aaf4945>.
  67. Srikant T, Drost H-G. 2020. How stress facilitates phenotypic innovation through epigenetic diversity. *Front Plant Sci* 11:606800. <https://doi.org/10.3389/fpls.2020.606800>.
  68. Vuković R, Liber Z, Ježić M, Sotirovski K, Ćurković-Perica M. 2019. Link between epigenetic diversity and invasive status of south-eastern European populations of phytopathogenic fungus *Cryphonectria parasitica*. *Environ Microbiol* 21:4521–4536. <https://doi.org/10.1111/1462-2920.14742>.
  69. Mishra PK, Baum M, Carbon J. 2011. DNA methylation regulates phenotype-dependent transcriptional activity in *Candida albicans*. *Proc Natl Acad Sci U S A* 108:11965–11970. <https://doi.org/10.1073/pnas.1109631108>.
  70. McLeod DV, Wild G, Úbeda F. 2021. Epigenetic memories and the evolution of infectious diseases. *Nat Commun* 12:4273. <https://doi.org/10.1038/s41467-021-24580-0>.
  71. Verhoeven KJF, Preite V. 2014. Epigenetic variation in asexually reproducing organisms. *Evolution* 68:644–655. <https://doi.org/10.1111/evo.12320>.
  72. Pappas PG, Kauffman CA, Andes DR, Clancy CJ, Marr KA, Ostrosky-Zeichner L, Reboli AC, Schuster MG, Vazquez JA, Walsh TJ, Zaoutis TE, Sobel JD. 2016. Clinical practice guideline for the management of candidiasis: 2016 update by the Infectious Diseases Society of America. *Clin Infect Dis* 62:e1–e50. <https://doi.org/10.1093/cid/civ933>.
  73. Lewis JS, II, Wiederhold NP, Wickes BL, Patterson TF, Jorgensen JH. 2013. Rapid emergence of echinocandin resistance in *Candida glabrata* resulting in clinical and microbiologic failure. *Antimicrob Agents Chemother* 57:4559–4561. <https://doi.org/10.1128/AAC.01144-13>.
  74. Singh-Babak SD, Babak T, Diezmann S, Hill JA, Xie JL, Chen Y-L, Poutanen SM, Rennie RP, Heitman J, Cowen LE. 2012. Global analysis of the evolution and mechanism of echinocandin resistance in *Candida glabrata*. *PLoS Pathog* 8:e1002718. <https://doi.org/10.1371/journal.ppat.1002718>.
  75. Perlin DS. 2015. Mechanisms of echinocandin antifungal drug resistance. *Ann N Y Acad Sci* 1354:1–11. <https://doi.org/10.1111/nyas.12831>.
  76. Proctor DM, Dangana T, Sexton DJ, Fukuda C, Yelin RD, Stanley M, Bell PB, Baskaran S, Deming C, Chen Q, Conlan S, Park M, NISC Comparative Sequencing Program, Welsh RM, Vallabhaneni S, Chiller T, Forsberg K, Black SR, Pacilli M, Kong HH, Lin MY, Schoeny ME, Litvintseva AP, Segre JA, Hayden MK. 2021. Integrated genomic, epidemiologic investigation of *Candida auris* skin colonization in a skilled nursing facility. *Nat Med* 27:1401–1409. <https://doi.org/10.1038/s41591-021-01383-w>.
  77. Chowdhary A, Anil Kumar V, Sharma C, Prakash A, Agarwal K, Babu R, Dinesh KR, Karim S, Singh SK, Hagen F, Meis JF. 2014. Multidrug-resistant endemic clonal strain of *Candida auris* in India. *Eur J Clin Microbiol Infect Dis* 33:919–926. <https://doi.org/10.1007/s10096-013-2027-1>.
  78. Rhodes J, Abdolrasouli A, Farrer RA, Cuomo CA, Aanensen DM, Armstrong-James D, Fisher MC, Schelenz S. 2018. Genomic epidemiology of the UK outbreak of the emerging human fungal pathogen *Candida auris*. *Emerg Microbes Infect* 7:43. <https://doi.org/10.1038/s41426-018-0045-x>.
  79. Perlin DS. 2015. Echinocandin resistance in *Candida*. *Clin Infect Dis* 61: S612–S617. <https://doi.org/10.1093/cid/civ791>.
  80. Sherrington SL, Sorsby E, Mahtey N, Kumwenda P, Lenardon MD, Brown I, Ballou ER, MacCallum DM, Hall RA. 2017. Adaptation of *Candida albicans* to environmental pH induces cell wall remodelling and enhances innate immune recognition. *PLoS Pathog* 13:e1006403. <https://doi.org/10.1371/journal.ppat.1006403>.



81. Nobile CJ, Solis N, Myers CL, Fay AJ, Deneault J-S, Nantel A, Mitchell AP, Filler SG. 2008. *Candida albicans* transcription factor Rim101 mediates pathogenic interactions through cell wall functions. *Cell Microbiol* 10: 2180–2196. <https://doi.org/10.1111/j.1462-5822.2008.01198.x>.
82. Fayed B, Jayakumar MN, Soliman SSM. 2021. Caspofungin-resistance in *Candida auris* is cell wall-dependent phenotype and potential prevention by zinc oxide nanoparticles. *Med Mycol* 59:1243–1256. <https://doi.org/10.1093/mmy/myab059>.
83. Ichikawa Y, Bruno VM, Woolford CA, Kim H, Do E, Brewer GC, Mitchell AP. 2021. Environmentally contingent control of *Candida albicans* cell wall integrity by transcriptional regulator Cup9. *Genetics* 218:iyab075. <https://doi.org/10.1093/genetics/iyab075>.
84. Blankenship JR, Fanning S, Hamaker JJ, Mitchell AP. 2010. An extensive circuitry for cell wall regulation in *Candida albicans*. *PLoS Pathog* 6: e1000752. <https://doi.org/10.1371/journal.ppat.1000752>.
85. Castillo L, Martínez AI, Garcerá A, García-Martínez J, Ruiz-Herrera J, Valentín E, Sentandreu R. 2006. Genomic response programs of *Candida albicans* following protoplasting and regeneration. *Fungal Genet Biol* 43:124–134. <https://doi.org/10.1016/j.fgb.2005.12.002>.
86. Healey KR, Perlin DS. 2018. Fungal resistance to echinocandins and the MDR phenomenon in *Candida glabrata*. *J Fungi (Basel)* 4:105. <https://doi.org/10.3390/jof4030105>.
87. Popp C, Hampe IAI, Hertlein T, Ohlsen K, Rogers PD, Morschhäuser J. 2017. Competitive fitness of fluconazole-resistant clinical *Candida albicans* strains. *Antimicrob Agents Chemother* 61:e00584-17. <https://doi.org/10.1128/AAC.00584-17>.
88. Hill JA, O'Meara TR, Cowen LE. 2015. Fitness trade-offs associated with the evolution of resistance to antifungal drug combinations. *Cell Rep* 10: 809–819. <https://doi.org/10.1016/j.celrep.2015.01.009>.
89. Kaiser C, Michaelis S, Mitchell A. 1994. *Methods in yeast genetics: a laboratory course manual*. Cold Spring Harbor Laboratory Press, Cold Spring Harbor, NY.
90. Clinical and Laboratory Standards Institute. 2008. Reference method for broth dilution antifungal susceptibility testing of yeast. Approved standard, CLSI document M27-A3. Clinical and Laboratory Standards Institute, Wayne, PA.
91. Reuß O, Vik Å, Kolter R, Morschhäuser J. 2004. The SAT1 flipper, an optimized tool for gene disruption in *Candida albicans*. *Gene* 341:119–127. <https://doi.org/10.1016/j.gene.2004.06.021>.
92. Tscherner M, Zwolanek F, Jenull S, Sedlazeck FJ, Petryshyn A, Frohner IE, Mavrianos J, Chauhan N, von Haeseler A, Kuchler K. 2015. The *Candida albicans* histone acetyltransferase Hat1 regulates stress resistance and virulence via distinct chromatin assembly pathways. *PLoS Pathog* 11: e1005218. <https://doi.org/10.1371/journal.ppat.1005218>.
93. Andrews S. 2010. FastQC: a quality control tool for high throughput sequence data.
94. Sedlazeck FJ, Rescheneder P, von Haeseler A. 2013. NextGenMap: fast and accurate read mapping in highly polymorphic genomes. *Bioinformatics* 29:2790–2791. <https://doi.org/10.1093/bioinformatics/btt468>.
95. Anders S, Pyl PT, Huber W. 2015. HTSeq—a Python framework to work with high-throughput sequencing data. *Bioinformatics* 31:166–169. <https://doi.org/10.1093/bioinformatics/btu638>.
96. Robinson JT, Thorvaldsdóttir H, Winckler W, Guttman M, Lander ES, Getz G, Mesirov JP. 2011. Integrative genomics viewer. *Nat Biotechnol* 29: 24–26. <https://doi.org/10.1038/nbt.1754>.
97. Robinson MD, McCarthy DJ, Smyth GK. 2010. edgeR: a Bioconductor package for differential expression analysis of digital gene expression data. *Bioinformatics* 26:139–140. <https://doi.org/10.1093/bioinformatics/btp616>.
98. Benjamini Y, Hochberg Y. 1995. Controlling the false discovery rate: a practical and powerful approach to multiple testing. *J R Stat Soc Series B Stat Methodol* 57:289–300. <https://doi.org/10.1111/j.2517-6161.1995.tb02031.x>.
99. Yu G, Wang L-G, Han Y, He Q-Y. 2012. clusterProfiler: an R package for comparing biological themes among gene clusters. *OMICS* 16:284–287. <https://doi.org/10.1089/omi.2011.0118>.
100. Chen H, Boutros PC. 2011. VennDiagram: a package for the generation of highly-customizable Venn and Euler diagrams in R. *BMC Bioinformatics* 12:35. <https://doi.org/10.1186/1471-2105-12-35>.
101. Nogueira MF, Istel F, Jenull S, Walker LA, Gow NA, Lion T. 2017. Quantitative analysis of *Candida* cell wall components by flow cytometry with triple-fluorescence staining. *J Microbiol Mod Tech* 2:101.
102. Chudzik B, Bonio K, Dabrowski W, Pietrzak D, Niewiadomy A, Olender A, Pawlikowska-Pawłęga B, Gagoś M. 2019. Antifungal effects of a 1,3,4-thiadiazole derivative determined by cytochemical and vibrational spectroscopic studies. *PLoS One* 14:e0222775. <https://doi.org/10.1371/journal.pone.0222775>.
103. Penninger P, Riedelberger M, Tsymala I, Arzani H, Jenull S, Kuchler K. 2021. Quantification of zinc intoxication of *Candida glabrata* after phagocytosis by primary macrophages. *STAR Protoc* 2:100352. <https://doi.org/10.1016/j.xpro.2021.100352>.
104. Riedelberger M, Penninger P, Tscherner M, Seifert M, Jenull S, Brunnhofer C, Scheidl B, Tsymala I, Bourgeois C, Petryshyn A, Glaser W, Limbeck A, Strobl B, Weiss G, Kuchler K. 2020. Type I interferon response dysregulates host iron homeostasis and enhances *Candida glabrata* infection. *Cell Host Microbe* 27:454–466.e8. <https://doi.org/10.1016/j.chom.2020.01.023>.
105. Zwolanek F, Riedelberger M, Stolz V, Jenull S, Istel F, Köprülü AD, Ellmeier W, Kuchler K. 2014. The non-receptor tyrosine kinase Tec controls assembly and activity of the noncanonical caspase-8 inflammasome. *PLoS Pathog* 10: e1004525. <https://doi.org/10.1371/journal.ppat.1004525>.
106. Frohner IE, Bourgeois C, Yatsyk K, Majer O, Kuchler K. 2009. *Candida albicans* cell surface superoxide dismutases degrade host-derived reactive oxygen species to escape innate immune surveillance. *Mol Microbiol* 71: 240–252. <https://doi.org/10.1111/j.1365-2958.2008.06528.x>.
107. RStudio Team. 2020. RStudio: integrated development environment for R. R Foundation for Statistical Computing, Vienna, Austria.